Inorganic Chemistry

pubs.acs.org/IC Article

Ligand-Nuclei Effects on Spin Relaxation in V(IV) Complexes

Published as part of Inorganic Chemistry special issue "Quantum Materials from an Inorganic Chemistry Perspective".

Roxanna Martinez, Ökten Üngör, Cassidy E. Jackson, Firoz S. T. Khan, Johan van Tol, and Joseph M. Zadrozny*

Cite This: *Inorg. Chem.* 2025, 64, 15588−15599 Read Online

ACCESS | Metrics & More | Article Recommendations | Supporting Information

ABSTRACT: Understanding how magnetic nuclei affect spin relaxation is vital for designing robust spin coherence in magnetic materials and molecules. A key question is the extent that magnetic nuclei close to a spin (e.g., in the ligand shell of a metal complex) influence relaxation and how it varies over different classes of nuclei. Herein, we apply high-field EPR, X-band EPR, and ac magnetic susceptibility techniques to a family of five V(IV) complexes of the type $[V(C_6X_4O_2)_3]^{2-}$, featuring five different sets of 12 nuclear spins on the ligand shell: X = ^{1}H (**1**), ^{2}H (**2**), ^{19}F (**3**), $^{35/37}$Cl (**4**), and $^{79/81}$Br (**5**). We found several unanticipated results in these studies. For example, at high-field/-frequency, we found that compound **1**, with the highest-magnetic-moment ligand nuclear spins, exhibits the longest phase memory relaxation times of the series. Furthermore, at lower fields, we found that the spin−lattice relaxation time and its field dependence were ligand-dependent, despite no obvious change in electronic structure across the five species. Based on this data, structural comparisons, and Raman spectroscopic data, we tentatively conclude that the spin−lattice relaxation properties of **1**−**5** stem from fine-tuning of the local magnetic environment with changing identity of the X atoms.

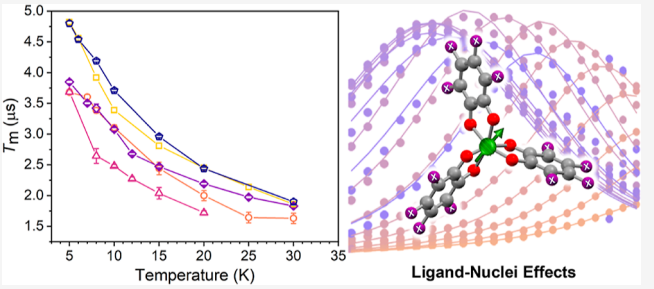

INTRODUCTION

Electron spin relaxation in open-shell molecules and magnetic materials is an important fundamental process. It dictates how long information can be stored in a spin's orientation, which is relevant for next-generation computational technologies.[1] It also governs whether sensing resolution in biomedicine is enhanced by sharp line widths.[2] For nearly all spin-based applications, the ideal spin relaxation process is slow, where the rate of this process is defined as the inverse of either the spin-lattice relaxation time (T_1) or the spin-spin relaxation time (T_m or T_2). Design strategies to lengthen T_1 and T_m are desperately needed for eventual application, and molecules are useful to determine these strategies owing to their high inherent chemical tunability.[3]

One key challenge in the design of slow relaxation is the impact of nearby magnetic species and the magnetic field fluctuations (or noise) they create, which generally hasten relaxation rates. We have shown that a dominant source for noise in an open-shell compound can come from functional groups on the molecule itself.[4−7] Separate proofs of concept demonstrate that elimination of nuclear spin entirely through favored composition of C, S, and O atoms can produce extremely slow relaxation.[8−12] But, it is worth noting these latter conditions are a far reach from the noisy, nuclear spin-rich environment of aqueous tissue or the magnetically noisy interior of an electronic device. Toward slow spin relaxation in more realistic application environments, we need a better picture of how chemistry creates noise.

There is some important nuance to the impact of magnetic noise on spin relaxation processes. Spin-spin relaxation is well-known to be hastened by nuclear spin diffusion, a process where a pair of resonant nuclei flip-flop and create noise.[13−17] Spin-lattice relaxation, however, is generally more dependent on thermal effects because this relaxation mechanism requires energy exchange with the vibrations of the surrounding lattice.[3,18,19] However, nearby magnetic units can still affect T_1, but these effects are largely confined to close electron-spin to electron-spin contacts that shorten T_1. In this respect, T_1 is like T_m, as both relaxation times increase as a given spin system is spatially separated from others, which is often accomplished by dilution in solution or through cocrystallization with a diamagnetic[20] (or effectively so)[21] analogue.

Received: April 29, 2025
Revised: July 7, 2025
Accepted: July 16, 2025
Published: July 24, 2025

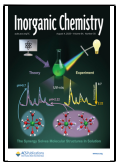

https://doi.org/10.1021/acs.inorgchem.5c01930
Inorg. Chem. 2025, 64, 15588−15599

Magnetic nuclei are relatively less explored for their effects on T_1. In part, this lack of information (in contrast to T_m) is because nuclear spin diffusion is generally not considered as an influential effect. At most, a magnetic nucleus on the same atom as an unpaired electron can affect T_1 by inducing quantum tunneling of the magnetization[1,22] at or near zero-field.[23,24] Generally, however, at a given field the Larmor frequencies of environmental magnetic nuclei differ so strongly from those of electron spins that nuclear spins are ignored in T_1 analyses.

We propose that this general picture of the effect of nuclei on electron spin relaxation is shortsighted. Magnetic nuclei have a diverse range of nuclear spin states and a diversity of quadrupolar couplings. These effects control the time scales of nuclear spin dynamics, with no theoretical "speed limit" for how fast nuclei can relax. Indeed, it is already established that the relaxation times of nuclei can approach the fast-time-scale dynamics of unpaired electrons. For example, quadrupolar Cl and Br atoms have relaxation times that preclude NMR analyses in solution for most organic compounds,[25] which imply T_1 times in the window of microseconds or faster, analogous to, e.g., organic radicals.[26] Hence, it is a reasonable expectation that nuclei could affect spins at the T_1 level not just at T_m. More chemical systems to test this hypothesis are needed.

Herein, we use V(IV) triscatecholate complexes to provide a test of the extent to which ligand-nuclei engineering can influence T_m and T_1. We use these species to produce a local environment with 12 ^{1}H, ^{2}H, ^{19}F, $^{35/37}$Cl, and $^{79/81}$Br nuclear spins around an $S = 1/2$ V(IV) spin center (Figure 1). We

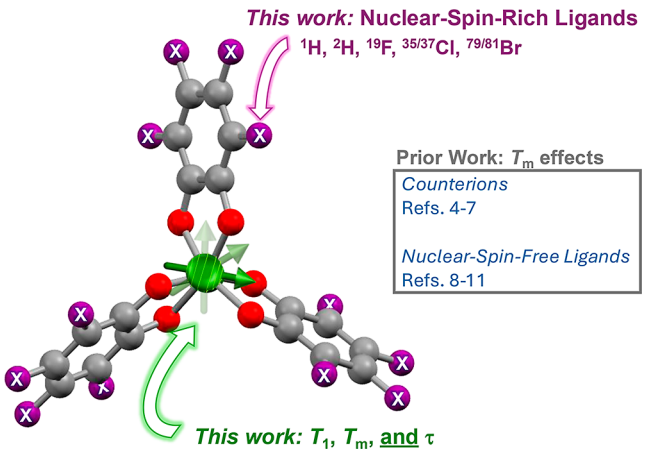

Figure 1. This paper investigates the role of ligand nuclear spins on the electron relaxation times (T_1, T_m, τ) in V(IV) complexes.

then applied pulsed electron paramagnetic resonance (EPR) spectroscopy and alternating-current (ac) SQUID magnetometry to investigate the impact of these magnetic nuclei on spin relaxation processes. Importantly, as part of these analyses, we show by SQUID magnetometry that the measured relaxation time τ, which approximates T_1 in this technique, is dependent on the ligand shell nuclei, which enables a fine-tuning of the local magnetic environment. This latter result is unique and expands the potential degrees of freedom that chemists can tune to control T_1.

EXPERIMENTAL SECTION

General Considerations. All manipulations and syntheses of **1**-**5** were performed under a N_2 atmosphere with either Vigor glovebox or Schlenk techniques. The complexes $(Bu_3NH)_2[V(C_6H_4O_2)_3]$ (**1**), $(Bu_3NH)_2[V(C_6Cl_4O_2)_3]$ (**4**), and $(Bu_3NH)_2[V(C_6Br_4O_2)_3]$ (**5**) were prepared following published procedures.[4,6,7] Glassware was flame dried before being brought into the glovebox. THF, toluene, and hexanes were dried using a commercial solvent purification system from LC Technology Solutions and were stored over 4 Å molecular sieves prior to use. Four Å molecular sieves were stored in a 150 °C oven and were activated at 280 °C under reduced pressure for at least 12 h prior to use. Catechol, catechol-d_6, tetrachlorocatechol, tetrabromocatechol, vanadyl acetylacetonate ($VO(acac)_2$), and d_{14}-*o*-terphenyl (OTP) were purchased from commercial suppliers and used as received. Tetrafluorocatechol was prepared following the literature procedures.[27]

Synthesis of $(n\text{-}Bu_3NH)_2[V(C_6D_4O_2)_3]$ (**2**). In a N_2-filled glovebox, a 20 mL scintillation vial was charged with 0.150 g (0.565 mmol) of $VO(acac)_2$, 0.197 g (1.69 mmol) of catechol-d_6, ca. 8 mL of THF, and a Teflon-coated magnetic stir bar. A solution of 0.197 μL (1.13 mmol) of *n*-Bu_3N was added to the mixture with gentle shaking, resulting almost immediately in an intensely dark blue solution. The reaction mixture was allowed to stir overnight. All volatile materials (THF, H_2O, and acetylacetone) were removed under reduced pressure. The resulting dark blue residue was washed twice with ca. 5 mL of cold Et_2O (Note: the complex is slightly soluble in Et_2O) and twice with ca. 4 mL of hexanes and then was dried under reduced pressure to yield 0.405 g of dark blue powder. The solid was further purified by slow evaporation of THF in the glovebox for 2 weeks to afford 0.383 g (0.512 mmol, 90% yield) of large, shiny, dark blue crystals suitable for single-crystal X-ray diffraction. Combustion analyses calculated for $C_{42}H_{65}D_{12}N_2O_6V$ (found): 67.45 (67.37) % C; 9.16 (9.18) % H; 3.75 (3.72) % N. LTQ-MS (m/z): positive ion mode: $\{n\text{-}Bu_3NH\}^+$, 186.22 (base); negative ion mode: $\{[V(C_6D_4O_2)_3]\}^-$, 388.27. IR (ATR, cm^{-1}): 2959, 2934, 2873, 2272, 1550, 1469, 1415, 1379, 1353, 1291, 1251, 1194, 1052, 1013, 923, 882, 844, 791, 612, 573, 528, 499, 422. UV−vis (CH_3CN); λ_{max}, nm (ε_M, M^{-1} cm^{-1}): 293 (15 000), 579 (8000), 684 (7200).

Synthesis of $(n\text{-}Bu_3NH)_2[V(C_6F_4O_2)_3]$ (**3**). In a N_2-filled glovebox, a 20 mL scintillation vial was charged with 0.110 g (0.412 mmol) of $VO(acac)_2$, 0.224 g (1.23 mmol) of tetrafluorocatechol, ca. 8 mL of THF, and a Teflon-coated magnetic stir bar. A solution of 195 μL (0.824 mmol) of *n*-Bu_3N was added to the mixture with gentle shaking, resulting almost immediately in an intensely dark blue solution. The reaction mixture was allowed to stir overnight. All volatile materials (THF, H_2O, and acetylacetone) were removed under reduced pressure. The resulting dark blue residue was washed twice with ca. 5 mL of cold Et_2O (Note: the complex is slightly soluble in Et_2O) and twice with ca. 4 mL of hexanes and then was dried under reduced pressure to yield 0.383 g of dark blue powder. The solid was further purified by slow evaporation of THF in the glovebox for 2 weeks to afford 0.375 g (0.400 mmol, 95% yield) of large, shiny, dark blue crystals suitable for single-crystal X-ray diffraction. Combustion analyses calculated for $C_{40}H_{52}F_{12}N_2O_6V$ (found): 51.34 (51.30) % C; 5.60 (5.57) % H; 2.99 (2.98) % N. LTQ-MS (m/z): positive ion mode: $\{n\text{-}Bu_3NH\}^+$, 186.22 (base); negative ion mode: $\{[V(C_6F_4O_2)_3]\}^-$, 590.89. IR (ATR, cm^{-1}): 3048, 2956, 2872, 1568, 1465, 1377, 1253, 1097, 1014, 870, 799, 733, 628, 537, 501, 412. UV−vis (THF); λ_{max}, nm (ε_M, M^{-1} cm^{-1}): 298 (15 000); 456 (3200); 575 (5200); 682 (4800).

X-ray Data Collection, Structure Solution and Refinement. Single-crystal X-ray diffraction data for **2** and **3** were collected at the X-ray diffraction facility at Cornell University. Data were collected and integrated using Bruker Apex 3 software.[28] Absorption corrections were applied using SADABS.[29] Space group assignments were determined by examination of systematic absences, *E* statistics, and successive refinement of the structures. Crystal structures were solved using SHELXT[30] and refined with the aid of successive difference Fourier maps by SHELXL[30] operated in conjunction with

https://doi.org/10.1021/acs.inorgchem.5c01930
Inorg. Chem. 2025, 64, 15588−15599

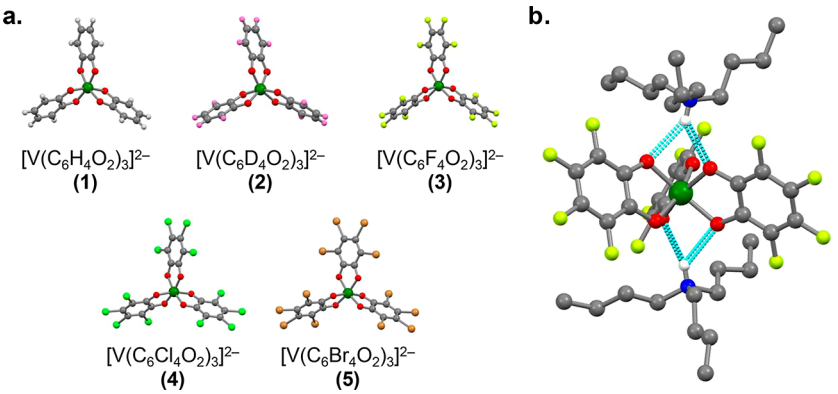

Figure 2. Overview of single-crystal diffraction results and molecular structure. (a) Molecular structures of $[V(C_6X_4O_2)_3]^{2-}$ complexes as determined from single-crystal diffraction experiments on **1**-**5**. Dark green, orange, bright green, yellow, red, gray, pink, and white spheres are V, Br, Cl, F, O, C, D (^{2}H), and H atoms, respectively. Counterions are omitted for clarity. (b) Depiction of the nBu$_3$NH$^+$ counterions' associations with $[V(C_6F_4O_2)_3]^{2-}$ seen from diffraction analysis of **3**. The depicted interaction is representative of the entire series of **1**-**5**. Molecular structures for **1**, **4**, and **5** were originally reported in refs 4,6, and 7.

OLEX2 software.[31] None of the crystals demonstrated decay by X-ray radiation over the course of the experiment. Hydrogen atoms were placed in ideal positions and refined using a riding model for all of the structures. Crystallographic information files for **2** and **3** are available in the CSD at accession numbers 2386040 and 2386039.

Electron Paramagnetic Resonance. All samples were prepared under an inert atmosphere. For high-frequency analyses at the National High Magnetic Field Laboratory, samples **1**−**5** were prepared at 1 mM concentration by first loading 40 μL 1 mM THF solution of **1** by a micropipette into a 4 mm OD quartz EPR tube. Following removal of THF under reduced pressure, 0.0516 g of d^{14}-*o*-terphenyl (40 μL when molten) was loaded into the same tube. These tubes were flame-sealed under dynamic vacuum (<50 mTorr) and placed in a 65-70 °C oil bath until a clear dark blue solution was formed. While sample tubes prepared in this manner can be stored at room temperature for an extended period without compound decomposition, the quality of glass appeared to decay with extended time. Hence, prior to each measurement, the samples were remelted and frozen. For X-band continuous wave measurements, samples were prepared in toluene at 1 mM and flame-sealed in 4 mm OD quartz tubes (Wilmad).

All continuous-wave EPR spectra were collected at the analytical resources core of Colorado State University with a Bruker ELEXSYS ESR-500 X-band CW EPR spectrometer. All pulsed EPR data were collected at the National High Magnetic Field Laboratory (NHMFL, Tallahassee, FL, USA). These data were collected on a custom built 120/240/336 GHz EPR spectrometer, operated at 120 GHz for the experiments in this paper.[32] Samples of **1**-**5** were gently melted using a heat gun to afford a homogeneous dark blue solution, then quickly inserted into the resonator to ensure glassing behavior of the OTP. Pulsed EPR data were processed using an EPR measurement program locally developed at NHMFL, Matlab,[33] and Origin Pro software packages.[34] Continuous-wave and echo-detected, field-swept EPR spectra were simulated using EasySpin.[35]

Spin−Lattice Relaxation Experiments and Analyses. T_1 data were collected on the most intense resonance of the Echo-detected field sweep (EDFS) spectra at 4.4 T at 120 GHz via an inversion recovery sequence (π−T−π/2−τ−π−τ−echo). The length of the three pulses, π−π/2−π, were 900−600−900 ns with a starting T value of 10,300 ns and τ of 700 ns. The inversion recovery data were fit by using a stretched exponential function:

$$I(\tau) = I(0) - Ae^{-\left(\frac{T}{T_1}\right)^{\beta}} \quad (1)$$

The temperature-dependent T_1 data were modeled with the following equation in Origin:

$$\frac{1}{T_1} = A_{\mathrm{Dir}}B^4T + A_{\mathrm{ram}}T^9 \quad (2)$$

where, T is the temperature, A_{dir} is the direct process coefficient, A_{Ram} is the Raman process coefficient, and B is the magnetic field. The exponent of 4 for B was chosen for consistency with analyses of other V(IV) systems, and the Raman exponent of 9 was fixed for a variety of reasons, primarily consistency with expectations for half-integer spins without low-lying excited states[18] and previous reports.[4,6,7] Further, note that models of the temperature dependence of T_1 that allowed the Raman exponent, "n", to refine produced equal quality fits with n varying from 2.0(4) to 8.8(6). Given the similarity of the complexes in terms of structure, electronics, and solvent, as well as the limited temperature window over which the Raman process appears influential, we thought it best to be cautious and restrain our reported fit parameters to the n = 9 case. Attempts to model T_1 with a local mode process resulted in fits with an unreasonably large uncertainty for a local mode energy; hence, we discarded that possibility as well.

Phase-Memory Relaxation Experiments and Analyses. T_m data at 120 GHz were collected on the most intense resonance (4.4 T) in the EDFS spectra via a Hahn echo sequence (π/2−τ−π− τ−echo) with microwave pulses of 600 (π/2) and 900 ns (π) and an interpulse time (τ) of 700 ns. Owing to the long pulse lengths and 100 ns deadtime on the 120 GHz spectrometer, T_m values below 200−300 ns were in general extremely difficult to observe; hence, all analyses generally stopped by 40 K.

Magnetic Measurements. Ac magnetic susceptibility experiments were performed on polycrystalline samples of **1**-**5** using a Magnetic Property Measurement System MPMS3 (Quantum Design). All samples were finely ground and restrained with eicosane to ensure good contact with the thermal bath and prevent crystallite torquing. Measurements were performed at 5 K with applied magnetic fields up to 7 T and ac field frequency ranging typically from 1 to 1000 Hz and applied static direct-current (dc) fields of up to a few tesla.

Raman Spectroscopy. Raman spectra were collected on microcrystalline powders of **1**-**5** loaded under an N_2 atmosphere into quartz tubes and sealed with small septa. Spectra were collected with either 633 nm (**1**-**5**) or 514 nm (ligands) incident light using a Renishaw inVia Raman confocal microscope at the Center for Chemical and Biophysical Dynamics (CCBD) of Ohio State University. Typical powers were 10%, all samples were inspected during measurement to avoid material burning from the laser irradiation. Finally, the longer-wavelength laser did not yield useful spectra for the pure ligands, necessitating the 514 nm laser. Raman spectra were calculated using density functional theory and the optimized geometries, as these methods have been successfully

https://doi.org/10.1021/acs.inorgchem.5c01930
Inorg. Chem. 2025, 64, 15588−15599

Table 1. Selected Average Interatomic Distances in 1-5

	compound[a,b]				
	1	2	3	4	5
V−O	1.938(20)	1.948(1)	1.943(10)	1.941(13)	1.942(13)
C−O	1.341(1)	1.339(3)	1.34(2)	1.329(4)	1.330(6)
C1−C2	1.417(7)	1.414(6)	1.409(2)	1.415(2)	1.42(2)
V···X[c]	4.55(1)	4.55(1)	4.77(1)	4.96(2)	5.04(1)
V···X[d]	6.03(2)	6.03(1)	6.401(1)	6.75(1)	6.91(1)
V···N[e]	3.95(1)	3.91(7)	3.83(2)	3.94(2)	3.94(1)
V···CH_3[f]	7.1(1.5)	6.7(8)	6.9(9)	6.5(9)	6.8(9)
V···V[g]	10.93(1)	8.98(1)	9.81(1)	9.75(1)	9.89(1)

[a]All bond distances are averaged from each structure and reported in Å. [b]Parameters for **1**, **4**, and **5** are taken from refs 4, 6, and 7. [c]Through-space distances to the 3 and 6 positions of the catechol ring. [d]Through-space distances to substituents at the 4 and 5 positions of the catechol ring. [e]Through-space distances to the hydrogen-bonded N atom of the $n$$Bu_3NH^+$ counterions. [f]Calculated for the V-to-C distance of the CH_3 groups on the hydrogen bonded counterions. [g]Nearest-neighbor distance.

applied to studying vibrations that influence spin dynamics in the past.[36] Full geometry optimizations were performed using the B3LYP[37−39] basis functional with a triple ζ valence basis set (DEF2TVZP) in Gaussian 16, Revision C.01[40] through the Ohio Supercomputer Center.[41] Countercations were included in the calculations; hence, the overall charge on the molecules was zero and spin multiplicities of 2 were used throughout owing to the V(IV) oxidation states. No imaginary frequencies were found for the optimized geometries during the frequency calculations. Molecular frameworks of the optimized geometries and their associated vibrations were visualized and drawn through ChemCraft.[42]

Other Physical Measurements. ^{1}H NMR spectra were collected on a Bruker Avance NEO 400 MHz spectrometer. The spectra were referenced using a residual protiated solvent signal as an internal standard ($CDCl_3$, 7.26 ppm). Combustion analyses were performed by Midwest Microlab (Indianapolis, IN, USA). Infrared spectra were recorded on a Bruker TENSOR II FTIR spectrometer. Electronic absorption spectra were recorded on acetonitrile solutions of **1**−**5** with a Shimadzu UV-2600i UV−vis spectrophotometer using air-free quartz cuvettes with a 1 cm path length. Linear trap quadruple mass spectrometry (LTQ-MS) measurements were performed on acetonitrile solutions of **1**−**2** with a Thermo-Finnigan LTQ LC/MS−MS instrument at the Central Instrument Facility (CIF) of the Colorado State University.

RESULTS

Syntheses and Structures. Preparation of the studied complexes proceeded generally in a straightforward manner by combining the ligands, $VO(acac)_2$, and the tri-n-butyl ammonia base and refluxing in solvent. All reactions produced dark, inky-blue solutions, likely attributable to an LMCT of the $[V(C_6X_4O_2)_3]^{2-}$ unit in the UV-vis spectra,[43,44] which is consistent across **1**-**5**. Compounds **1**, **4**, and **5** are previously reported[4,6,7] while compounds **2** and **3** are here reported for the first time.

Single-crystal diffraction experiments for **2** and **3** are discussed here alongside previously reported **1**, **4**, and **5** for completeness in the series. All species are six-coordinate, slightly distorted octahedral complexes with two hydrogen-bonded n-Bu_3NH^+ countercations (Figures 2, S1 and S2). Specific metrics are given in Tables S1 and S2. Average V−O bond lengths for **1**-**5** range from 1.938(20) (for **1**) to 1.948(1) Å (for **2**). Within the catechol ligand shells, C−O distances range from 1.329(4) for **4** to 1.34(2) Å for **3**, and the intradiol C_1−C_2 distances range from 1.409(2) for **3** to 1.417(7) Å for **1**. These V−O distances are consistent with a V(IV) oxidation state[45] and C−O and C−C distances are consistent with the catecholate redox state of the ligand shell.[46] Hence, we can safely rule out any redox noninnocence by the ligands in these species. Furthermore, the consistency in the V−O distances across **1**-**5** suggests the lack of any induced redox activity of V by the various ligand substituents. In summary, we can conclude that all metal ions in **1**-**5** are V(IV) ions, a conclusion that is supported by the spectroscopic data given below.

Each V(IV) ion in **1**-**5** has a unique magnetic environment dictated by the differing arrangements and placements of magnetic nuclei in the local vicinity of each V(IV) ion. Each catecholate ligand has two sets of equidistant sites to the V(IV) ion, the 3, 6 and 4, 5 positions, where ^{1}H, ^{2}H, ^{19}F, $^{35/37}$Cl, and $^{79/81}$Br magnetic nuclei are placed. Furthermore, each $[V(C_6X_4O_2)_3]^{2-}$ complex is accompanied by two hydrogen-bonded counterions. This interaction generates V···N distances near 4 Å, and since each n-Bu_3NH^+ cation has three CH_3 groups, there are additional V···CH_3 distances that range from 6.5 to 7.1 Å. Finally, at least in the crystal structure, each complex has nearest neighbor compounds, with average V···V distances of 9 Å or greater. A summary of these distances is presented in Table 1. CH_3 groups are well-known to affect relaxation times,[5,7,47] as are closest-contact distances between paramagnetic metal ions.[3]

The changing ligand nuclei of **1**-**5** also modify the volumes of the complexes, as exemplified by the changing V···X distances across the series. The volumes of the unit cells from these experiments are 4927.9(7), 6234.8(7), 4558.6(5), 2575.3(4), and 5495.0(5) Å^3 for **1**-**5**, respectively. These volumes do not directly trend with the size of the molecules because of the changing crystal systems and solvents of crystallization. Nevertheless, these unit cells enable us to calculate the density of V(IV) spins in the crystalline lattice. These values for **1**-**5**, respectively, are 1.22(3), 0.96(2), 0.88(3), 0.78(7), and 0.72(2) V(IV)/nm^3. These calculated spin densities decrease with increasing X atom mass, likely reflecting the longer V···X distances, and the result is that crystals of complexes with heavier X atoms have a smaller V(IV) ion density.

Continuous-Wave and Echo-Detected EPR Spectra. Continuous-wave and echo-detected, field-swept EPR spectra were recorded on **1**-**5** to study how the ligand nuclei influence the electronic structure of the molecule (Figures 3 and S3−S5). Continuous-wave measurements were conducted in both solution and the solid-state using X-band (ca. 9.46 GHz) frequency. Echo-detected spectra were collected with high-field/high-frequency (ca. 120 GHz) microwaves for **1**-**5**. The X-band solution and solid-state spectra show 8-line patterns

https://doi.org/10.1021/acs.inorgchem.5c01930
Inorg. Chem. 2025, 64, 15588−15599

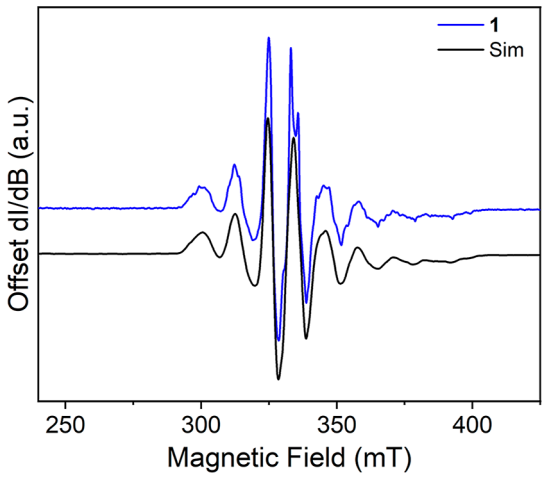

Figure 3. Frozen-solution X-band continuous-wave EPR spectrum of **1** (blue) at 77 K and simulation (black). Experimental details: 1 mM solutions; 0.63 microwave power; microwave frequency, ca. 9.46 GHz; modulation frequency, 100 kHz; modulation amplitude, 1.0 G; number of scans ranged from 10 to 15 to obtain good signal-to-noise ratios.

that span ca. 100 mT, representative of hyperfine coupling of the $S = 1/2$ V(IV) to the $I = 7/2$ ^{51}V nucleus. The 120 GHz echo-detected spectra, in contrast, show a single broad transition near 4.4 T. The enhanced effect of g anisotropy and g strain in the frozen solution leads to broad spectra at high field,[48] which precludes direct observation of the hyperfine splitting in the 120 GHz spectra, though the accuracy of the g anisotropy is still relatively high.

Simulations of all collected EPR spectra were performed with EasySpin[35] to extract the g_e and A values for **1-5** from the following spin Hamiltonian:

$$\hat{\boldsymbol{H}} = \mu_B \boldsymbol{B} \boldsymbol{g}_e \hat{\boldsymbol{S}} - \mu_N \boldsymbol{B} \boldsymbol{g}_N \hat{\boldsymbol{I}} + \hat{\boldsymbol{I}} \boldsymbol{A} \hat{\boldsymbol{S}} \quad (3)$$

In eq 3, $\boldsymbol{g}_e$ and $\boldsymbol{A}$ correspond to rhombic electronic g factors and ^{51}V hyperfine coupling constants, respectively. $\hat{\boldsymbol{S}}$ and $\hat{\boldsymbol{I}}$ are electronic and nuclear spin operators, respectively, and μ_B and μ_N are the respective Bohr and nuclear magnetons, respectively. Finally, $\boldsymbol{g}_N$ is the nuclear g factor for ^{51}V and $\boldsymbol{B}$ is the magnetic field.

In both solution and the solid state, the resulting simulations for the data collected at X-band and 120 GHz reveal similar g and A values for **1-5**. These extracted parameters do not vary substantially in magnitude and anisotropy as a function of the X atom on the ligands from the solid-state samples (Tables S3–S5). The general anisotropies and magnitudes of g and A for **1-5** suggest the lone electron occupies a d_{z^2} orbital, consistent with literature observations on trigonal prismatic V(IV) ions[8,49−54] and triscatecholate V(IV) complexes.[55] Furthermore, the consistency of the obtained g and A values indicate sharply similar electronic structures for V(IV) in **1-5**, with no substantial changes in spin delocalization onto the ligands with different X atom functional groups.

The solution-phase CW spectra exhibit slight differences in line width between **1-5**. Complex **1** has the sharpest peak-to-peak line width (18 G), while complex **5** exhibits the broadest line widths (26 G), see Figure S5. Simulations with EasySpin's garlic function show successful simulation with similar g and A values as the frozen solution data. This function also enables simulation of line width based on a correlation time, τ_{corr}, the time for a complex to rotate one radian. The extracted τ_{corr} values range from 401 to 473 ps for **1-5**. Interestingly, the correlation time increases with the addition of heavier atoms on the ligands, from 406 ps for X = ^{1}H, to 413 ps for X = ^{2}H, to 420 ps for X = ^{19}F, 427 ps for X = $^{35/37}$Cl, and finally 430 ps for X = $^{79/81}$Br. Prior work in our group evaluated the effect of changing R_3NH^+ counterion mass/size on rotational correlation times for $[V(C_6H_4O_2)_3]^{2-}$.[7] There, CW EPR spectra showed a change in the correlation time of about 200 ps with a change in mass of 500 g/mol from Et_3NH^+ to n-Oct_3NH^+. In **1-5**, the mass change in the complexes is much higher, varying by nearly 960 g/mol as a function of X atom, but the change in correlation time is smaller, only ca. 70 ps. We attribute this weaker sensitivity to the fact that despite the larger mass variation across **1-5** compared to the counterion series, changing the X atom on the ligands causes a smaller change to the radius of the species relative to R_3NH^+. As a result, according to the Stokes–Einstein equation, the effect of changing the X atoms would have a weaker impact on rotation.[56]

Phase-Memory Relaxation by Hahn Echo. The phase-memory relaxation times, T_m, for **1-5** were collected by 2-pulse Hahn-echo experiments to study the impact of the different ligand nuclear spins. We performed two-pulse Hahn-echo experiments at the field of highest echo intensity (ca. 4.4 T, Figures 4, and S6–S10). Echo intensities generally decay with

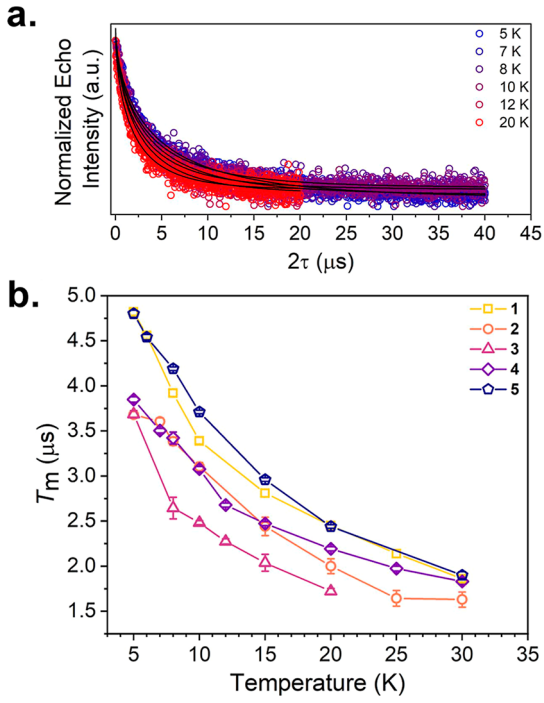

Figure 4. (a) Selected variable-temperature Hahn-echo decay curves (color traces) and fits (black traces) for **3**. (b) Variable-temperature T_m data for **1-5**. Data were collected at 120 GHz frequency on samples of ca. 1 mM concentration o-terphenyl-d^{14} glass.

increasing interpulse time, fading away completely by 40 μs at 5 K, but decay faster as temperatures increase. Echo decay curves were collected until about 30 K for all complexes. Above this temperature the long pulses ($\pi/2$ = 600 ns) and short relaxation times made it challenging to observe an echo.

Extraction of T_m from the echo decay curves was performed by fitting the decays with a stretched exponential function:

https://doi.org/10.1021/acs.inorgchem.5c01930
Inorg. Chem. 2025, 64, 15588−15599

$$I(\tau) = I(0) - Ae^{-\left(\frac{2\tau}{T_m}\right)^{\beta}} \quad (4)$$

where, β is the stretch parameter describing the shape of the echo decay.[5,18,47,56] Values of T_m and β are given in Table S8. The low temperature data were better fit with a stretched exponential equation due to the dominant nuclear spin diffusion. We found that β approaches 1 as the temperature increased, indicating that a conventional single exponential fit could be used. Nevertheless, we used the stretched exponential fit throughout the whole temperature range for consistency.

T_m values collected in this manner are around 3- μs at 5 K for all complexes and then decrease with increasing temperature. There are a few notable observations we make here. First, **1**, which contains ^{1}H nuclei on the ligand shell, exhibits the longest T_m at low temperature, as does **5**, which contains $^{79/81}$Br nuclei. This observation is notable because of the large nuclear magnetic moment on ^{1}H, which generally shortens the T_m. In that context, it is further interesting that **2** and **4**, which contain deuterons or Cl, respectively, show a faster relaxation than **1**, since ^{2}H and $^{35/37}$Cl possess smaller nuclear magnetic moments. Indeed, deuteration is a common strategy to lengthen T_m,[26] and a recent chlorinated radical also exhibited prolonged, >100 μs T_m constants, though at lower magnetic fields.[57] Finally, fully fluorinated **3** shows the shortest T_m at 5 K and the fastest relaxation over all measured temperatures. Despite our best attempts to find one, T_m of **1-5** does not show a clear trend in relation to the nuclei or any specific nuclear-spin properties.

Spin-Lattice Relaxation by Inversion Recovery. Temperature-dependent T_1 times were collected on **1-5** by inversion-recovery experiments to gain understanding of the operative spin-lattice relaxation processes (Figures 5, and S11–S15). For all complexes, the echo recovered after an initial π pulse over a time scale of ca. 1 ms. That time scale hastened with increasing temperature, and recovery was typically complete by 0.03 ms at the highest temperatures we could measure.

We extracted the T_1 parameters by fitting the echo recovery curves to a stretched exponential. T_1 varied between 1.23(5) and 0.09(2) ms from 5 to 30 K for complex **1**, decreasing with increasing temperature. Compound **3** was the fastest relaxing, with T_1 varying from 1.0(4) to 0.07(4) ms over the measured temperature range. Compound **4** had the shortest T_1 at 5 K (ca. 0.46 ms). Compounds **1**, **2**, **3**, and **5** had a T_1 of 1.23(5)-0.8(2) ms at 5 K. The T_1 times we report here are generally similar across the series and, importantly, to other V(IV) complexes that are previously reported.[8,58−64]

Analysis of the temperature dependence of T_1 (or the rate, $1/T_1$) enables a deeper look into the operative spin-lattice relaxation processes in **1-5** (Figure 5). In prior experiments on $[V(C_6H_4O_2)_3]^{2-}$ salts, we found that, at these temperatures and frequencies, spin-lattice relaxation was primarily driven by the direct process.[4,6,65] We found that the data for **1-5** were readily modeled using a sum of direct and Raman processes (see Experimental Section, Figure 5), in agreement with those prior findings. The T_1 varies slightly at 5 K between the complexes, with **4** having the shortest T_1. Yet, the T_1 times, at least, at these temperatures and frequencies, are relatively similar between the complexes. In comparison, other Cu(II)[66] and V(IV)[63] complexes can exhibit T_1 times that vary by an order of magnitude or more with ligand variation.

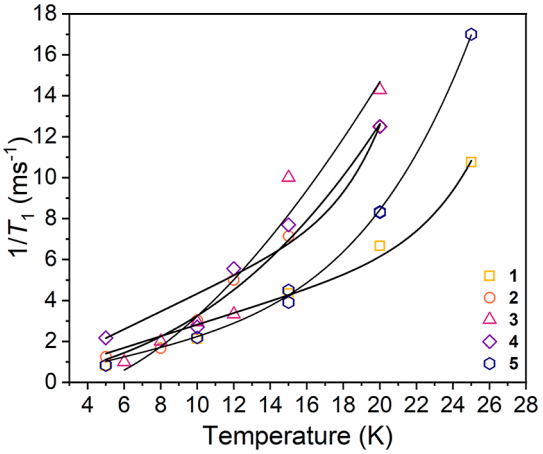

Figure 5. Temperature dependence of the spin-lattice relaxation rate ($1/T_1$) for **1-5**. Simulation of the temperature dependence is given as a black trace. Approx. field of acquisition was 4.4 T, the microwave frequency was 120 GHz, and samples were 1 mM in *o*-terphenyl-d^{14}. Fitting parameters and exact T_1 values are tabulated in the Supporting Information. Data for **1**, **4**, and **5** were originally reported in refs 4 and 6.

Spin-Lattice Relaxation by Alternating-Current (ac) Magnetic Susceptibility. Ac magnetic susceptibility measurements were performed on pure, microcrystalline samples of **1-5** at 5 K and variable fields as an additional test of the influence of ligand nuclear spins on V(IV) spin dynamics (Figures 6, and S16–S20). All species exhibited a featureless trace of χ_M'' versus ν under zero applied field. However, for all complexes, a peak appeared upon the application of a magnetic field. With increasing field, the peak would increase in intensity for **1-5** until about 1.5 T. At higher fields, the peak would begin to decrease in intensity. Throughout, the peaks would move from high to low ν before reversing course and moving to high ν again with increasing field. Compounds **1-5** all behaved similarly in this respect, however, the extent of the field dependence varied with compound identity. Compound **1** showed the greatest variation of χ_M'' intensity as a function of field, whereas **3** showed the largest change in ν of the peak. Compounds **1** and **2** exhibited remarkably similar field dependences of their ac data. The peaks of the χ_M'' data are inversely proportional to τ, the effective T_1 from the ac susceptibility measurement, indicating differing field-dependent relaxation dynamics for **1-5**.

Simulations of the χ_M'' versus ν traces allow us to quantitate the field dependence of the relaxation time. All complexes showed a short τ at low field and longer τ at higher field, in agreement with the field-dependent peak positions in the ac measurement. However, the slowing of the relaxation times with the field was starkly different. Compound **4** had the sharpest increase in τ, from 3.3(1) ms to 26(4) ms from 0 to 1.5 G, followed by compound **3**, which had an increase in τ from 0.07(2) to 4.8(2) ms from 200 G to 1.5 T. Compound **4** had the highest τ, of 26 ms at 1.5 G. Compound **1** showed the lowest general field dependence, with τ changing from 1(2) ms to 1.25(3) ms over the field window of the measurement. At the highest fields (up to 3.8 T), the τ values all dropped for **1-5**. Compound **4** had the sharpest drop off, from 15(4) ms at 2 T to 2(1) ms at 3.8 T. The observed values at high field, are, by and large, similar to the T_1 data collected by EPR, which were all measured at 4.4 T, beyond this window. The curvature

https://doi.org/10.1021/acs.inorgchem.5c01930
Inorg. Chem. 2025, 64, 15588−15599

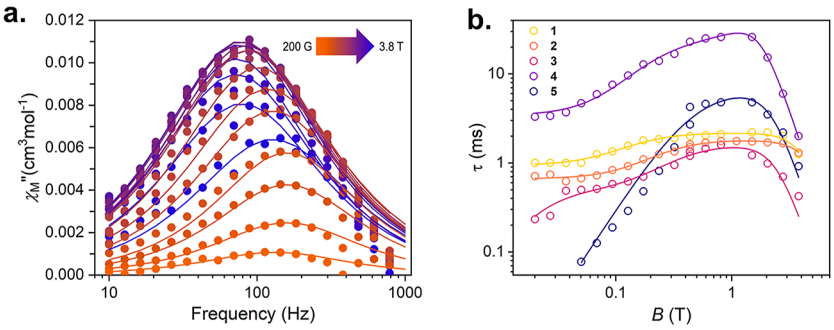

Figure 6. (**a**) Frequency dependence of the out-of-phase component χ_M'' of the magnetic susceptibility of **1** as a function of the magnetic field (200 G−3.8 T range) at 5 K. (**b**) Magnetic field dependence of τ extracted from ac magnetic susceptibility measurements for **1**−**5**. Colored lines depict best simulations of the data using the Brons-van-Vleck equation.

of τ vs the field plot suggests direct-process domination of T_1 at these high fields for this specific ion.

The field dependence of τ for **1-5** was modeled with the Brons-van-Vleck formula,[67] which accounts for the influence of the local environment on the relaxation time:

$$\tau^{-1} = cB^4 + d\left(\frac{1 + eB^2}{1 + fB^2}\right) \quad (5)$$

The first term of eq 5 corresponds to the direct mechanism of relaxation, which accelerates relaxation at higher magnetic fields B. The coefficient for this process, c, relates to the efficiency by which the spin system can eject energy from relaxation into the bath of lattice vibrations. The second term is more complex.[68−70] The parameter d is the zero-field relaxation rate, and both e and f relate to the internal magnetic field felt by the V(IV) spin (more on these definitions later). Qualitatively, the first term for the direct process is responsible for the shortening of τ at a high field, while the second term describes the lengthening of τ with increasing B at lower magnetic fields. Competition between these two rates leads to the observed plateauing behavior in $\tau(B)$.

Values of the best fits of the τ data from Figure 6 are given in Table 2. We found several correlations between these parameters and our observed data. The parameter c, which describes the onset of direct process relaxation, is largest in **5**, and appears to roughly scale with the weight of the ligands from **1**−**5**. This trend also reflects the generally sharper drop in τ at higher field with **1-5**. Parameter d, the zero-field relaxation rate, does not trend in any noticeable way across the compounds. In contrast, e and f, which connect to the internal field felt by the spin, both trend but do so in different ways. Parameter e drops from **1** to **5**, while f increases. Generally, the values we extracted are within the known range of reported parameters for V(IV) complexes studied by variable-field ac magnetometry.[58,59,61,63,64,71]

Table 2. Best-Fitted Parameters of Variable-Field τ Data for 1-5 with the Brons-van-Vleck Equation[a]

	c (T^{-4} ms^{-1})	d (ms^{-1})	e (T^{-2})	f (T^{-2})
1	1.35(2)	1.06(5)	29.6 (7)	65(19)
2	1.41(1)	1.51(1)	18.1(2)	50.0(6)
3	1.58(2)	2.32(4)	17.4(2)	58(9)
4	1.76(2)	0.248(3)	11.8(2)	90.4(24)
5	5.21(4)	6.37(2)	5.71(2)	220(22)

[a]All data were collected at 5 K.

Raman Spectroscopic Measurements. Recent connections between Raman-active vibrations and spin-lattice relaxation times[60−62,72−75] motivated us to explore the vibrational spectroscopy of **1-5** to better understand the low-temperature T_1 and τ data. All complexes are a deep, inky color owing to intense, overlapping charge-transfer bands at ca. 570 and 680 nm. Therefore, resonance Raman spectra were collected for **1-5** using a 633 nm red laser powered at 10% from 100 to 2200 cm^{-1} (Figures 7, and S22). Alongside **1-5**, we collected Raman spectra for the unbound catecholate ligands for **1-5** to facilitate comparison (Figure S23).

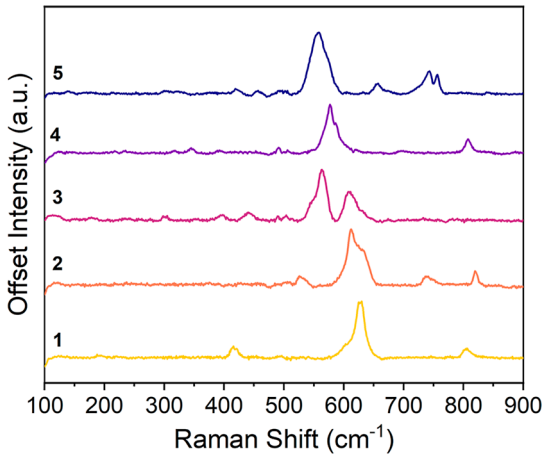

Figure 7. Resonance Raman spectroscopy results. Spectra of **1-5** were collected at 633 nm. All spectra were collected on powder samples at room temperature.

The spectra of **1-5** reveal multiple distinct peaks over the range of 150 to 1450 cm^{-1}. Spectra of **1-5** all show sharp vibrations at 558-625 cm^{-1} that appear to move to a lower wavenumber with a larger X atom (Figure 7). At a lower energy (below ca. 500 cm^{-1}), the peaks for **1-5** are weaker in intensity than higher energy peaks. Peak positions in the ligand spectra do not directly align to any of the peaks in the complexes. Complex **3** shows what looks like the lowest number of low energy vibrations. The ligands of **3-5** had the fewest peaks and lowest intensity in comparison to catechol and deuterated catechol. Overall complexes **4** and **5** tended to have broader peaks in comparison to those of **1-3**.

Comparison of these spectra with known analyses of VO_n complexes allows some conclusions to be made about the observed peaks. First and foremost, the sharp peak near 600

https://doi.org/10.1021/acs.inorgchem.5c01930
Inorg. Chem. 2025, 64, 15588−15599

cm^{-1} is like a symmetric VO stretching frequency. Wachs and Hardcastle studied these V−O stretches in depth as a function of bond distance and oxidation state.[76] Our average V−O bond distances in all complexes ranged from ca. 1.94 to 1.95 Å, and the strong observed peaks at ca. 600 cm^{-1} are in excellent agreement with the predicted value for those bond distances. If this assignment is true and if the consistency in our EPR and UV−vis spectra evidence a nearly consistent V(IV) electronic structure across **1-5**, then the Raman spectra depict a ligand-X atom-based kinematic impact on the V−O stretches, since the frequency of this shift seems to track with the increasing formula weight of the ligand shell. There is a notable absence of sharp, low-frequency peaks in **1-5** despite the observation of such signals in the spectra of the pure ligands (Figure S23). Yet, the two spectra were collected with different laser sources (514 nm for the ligands, 633 nm for **1-5**), and the longer-wavelength laser for **1-5** directly excited the LMCTs for these complexes. So, we tentatively propose that these key spectral differences likely reflect a decoupling of the very-low-energy ligand-based vibrations from the LMCT.[77]

Finally, we note the splitting of the assigned V−O stretches near 600 cm^{-1} for **3**, which appears anomalous relative to **1**, **2**, **4**, and **5**. We calculated the Raman spectra of **1**−**5** by using their optimized geometries to see if a simple explanation for this behavior would become evident. The calculated Raman spectra align quite closely with the experimental peaks observed (Figures S24−S28) and replicate the seemingly anomalous splitting of the 570-630 cm^{-1} peak for **3**. This correspondence also holds when the peaks are deconvoluted (Figure S29 and Table S9). However, a simple relation between the splitting of the vibrations and the X atom functional groups is not immediately apparent. Indeed, simulations of the motions of these V−O vibrations for **1-5** are all complex movements, incorporating bending motions of the ligands, changes to bite angles, and movement of the C−O bonds in addition to a component that is the V−O stretch. For **3**, the two peaks that appear correspond to a symmetric pinching motion of the O−V−O bite (583 cm^{-1}) while the higher-energy peak (683 cm^{-1}) incorporates a motion that appears closer to a simple V−O stretch (Figure S30). The complicated nature of the spectra precludes any obvious connection between vibration type and observed relaxation dynamics. Nevertheless, the simulations provide key evidence that the splitting of the VO stretch is a reasonable observation for **3** and not evidence of, e.g., an impurity also featuring V−O bonds.

DISCUSSION

The spin dynamics observations (in terms of T_m, T_1, and τ) for **1-5** have important implications for interpreting the role of ligand nuclei in spin relaxation. We will discuss T_m first, then T_1 and τ.

The observations from the Hahn-echo experiments on **1-5** are exciting because of their nonintuitive outcomes. Deuteration, either of solvents or the molecule itself, is one of the most common means of lengthening T_m for molecular spins.[8,10,78] The role of the deuteration is largely attributed to the smaller magnetic moment of the deuterium nucleus (0.86 μ_N) relative to that of the proton (2.79 μ_N), which affords weaker local magnetic noise and prolongs the spin coherence. Yet, if magnetic moments of the ligand X nuclei alone were responsible for the observed T_m trends, then we would see T_m values for **2** extend past **1** under our measured conditions. We would presumably also see a similar lengthening for **4** and **5** because the $^{35/37}$Cl and $^{79/81}$Br nuclei also have nuclear magnetic moments smaller than those of ^{1}H. That we do not see this effect implies that other factors also govern the V(IV) T_m at these high fields and frequencies.

A separate feature of magnetic nuclei that could be important for influencing the V(IV) T_m values is the intrinsic spin relaxation times of the nuclei themselves. We do not currently have an estimate of the T_1 times of the ligand nuclei in **1-5**. We can estimate the T_1 for ^{1}Hs to be less than 21 ms in solution, at room temperature, on the basis of the 0.19 ppm line widths seen in the 400 MHz ^{1}H NMR spectra for some of these complexes.[6,7] We cannot, however, extend this analysis across **1-5** because of the impossibility of measuring the solution-phase nuclear $T_{1,n}$ of the Br and Cl nuclei. Indeed, these strongly quadrupolar nuclei make NMR analysis challenging even in closed-shell systems, precisely because of the short $T_{1,n}$ values.[25] We anticipate that interactions with the V(IV) ion could make them even shorter. What we can say, importantly, is that **4** and **5**, with the strongly quadrupolar nuclei, do not together stand out relative to **1**, **2**, and **3** with short or long T_m values, which seems to rule out an effect, at least at the fields/temperatures of measurement.

At this point, we lack definitive evidence for a singular mechanism dominating the T_m. Our structural data show strongly similar molecular structures between **1-5**, especially in the distances to nearby magnetic species, e.g., CH_3 groups. This similarity suggests that the magnetic environments induced by nearby V(IV) ions and the Bu_3NH^+ counterions are largely similar, even in frozen solution. This similarity leaves the magnetic environment imposed by ligand shells in **1-5** as the lone changing variable. At the same time, our ac susceptibility and high-field pulsed EPR measurements point toward a short T_1 at the fields and temperatures of the Hahn-echo measurements. In this field-temperature regime, T_1 may be a convoluting factor in interpreting the mechanisms driving T_m in **1-5**. Hence, lower frequency/field studies to better understand the impacts of these nuclei on electron spin relaxation are ongoing. Furthermore, a recent preprint suggests that 1 mM concentrations (the sample concentrations of this study) in crystals are at the border of the electron- and nuclear-spin-dominated decoherence processes.[79] If true, even in the solvent glass of our measurements here, this situation would further convolute the processes, which motivates future concentration effects to be investigated in deeper detail.

The final effects that are perhaps most interesting are the trends in T_1 with the temperature and field across **1-5**. The temperature dependence of spin-lattice relaxation is highly dependent on the electronic structure of the relaxing spin and its local environment.[3] As described previously, the physical structures are essentially identical between **1-5**. Hence, the lack of stark variation in the T_1 temperature dependence for **1-5** (and similar series of complexes[4,6]) in the 120 GHz EPR measurements is likely attributed to the similarity in electronic structure (from the UV-vis and CW-EPR results), physical structures (from X-ray diffraction), and similarity in the concentration/solvent used.

The low- and high-field variation in T_1 (or τ) for solid samples of **1-5** are the only magnetic data that appear to evidence a meaningful trend. From the Brons-van-Vleck analysis, the high-field contribution of the direct process appears to increase with the size of the ligand X atom. The efficiency of the direct process increases with an increased

https://doi.org/10.1021/acs.inorgchem.5c01930
Inorg. Chem. 2025, 64, 15588−15599

density of low-frequency vibrations,[80] which may be molecular but also can be delocalized lattice phonons. In **1-5**, we therefore tentatively propose that the increasing mass of the ligand X atoms allows for a denser bath of low-energy lattice vibrations to facilitate the direct process for **5** over **1**, which would be consistent with the shift in the V−O stretch with increasing X atom mass, although those specific vibrations are likely too high in energy to influence these systems. We note our careful attention to sample preparation to avoid extrinsic phonon bottleneck effects that are sometimes seen in these types of measurements.[58]

At low field, we find a different variation in τ with a magnetic field. Here, τ increases with B for **1-5** and the magnitude of that increase trends from **1-5**. The two parameters, e and f, in the second term of eq 5 exhibit the greatest variation, and these parameters directly relate to the local magnetic environment felt by the relaxing V(IV) spin.[68−70] These measurements were performed on microcrystalline powders of **1-5**. Therefore, the similarity in the structures of the diffraction experiments, including the V···V and V···CH_3 distances, is directly relevant for the τ values. But here again, these structural parameters do not vary across **1-5** in a way that reflects any trend in the Brons-van-Vleck analysis.

The one parameter that does trend with the X atom is the local spin concentration determined from the single-crystal structure. We therefore tentatively conclude that the bulk of these data evidence that the changing of the ligand X atoms in **1-5** influences the low-field τ values not specifically by nuclear-spin effects but by small structural tuning of the V(IV) density in the crystals. This interpretation was somewhat challenging to arrive at based on conflicting literature descriptions of the meaning of the terms d, e, and f, if any, where the Brons-van-Vleck equation is applied. On top of that, attempts to physically quantify how explicit numerical changes in e and f directly correlate to molecular features in a given system are also absent, except for an excellent work on impact of crystallite size[58] and potential effects from cross relaxation.[63] Our own interpretation of the terms of d, e, and f comes from ref 68.

Note that both e and f appear to trend from **1-5**, but in opposite ways. An e that represents solely the inverse of the square of the internal magnetic field is consistent with our observations of the decreasing spin density in the crystal structures from **1**−**5**. This effect may reflect the relative importance of the local magnetic field on τ at low field: the weaker internal magnetic field from the lower spin-density crystals could be completely disrupted by a 0-to-1 T field, while the stronger internal fields of the higher spin density crystals are not. The second point, the f term, appears to vary in the opposite way, which should not be the case if both e and f depended on the local magnetic field in the same way. Ultimately, more studies are needed to determine what molecular parts dictate the values of these parameters.

Note that the Brons-van-Vleck equation does not specifically account for the spin dynamics of the species generating the local magnetic field, which we established above are likely vital to understanding the system and may be related to f. Indeed, only recently was a model published that attributed the low-B increase in τ (in part) to spin noise and T_m of the relaxing spin system.[81] As T_m can be influenced by proximate magnetic nuclei, this model may hint that ligand-based nuclear spins could influence V(IV) τ. Ultimately, however, future experiments will be necessary to map out exactly what electronuclear interactions could do so. In this case, the slight variation in the crystalline spin density as a function of the X atom is a compelling match for the role of lattice tuning on the parameter e and the field dependence of τ.

CONCLUSION

Understanding how local environment affects a metal ion's spin dynamics is a vital step toward exploiting these species for any spin-based application. Herein, we present a study of six V(IV) complexes by spectroscopic and magnetometric methods that shows how differing monatomic functional groups on ligands can influence spin-relaxation processes. We note that magnetic nuclei at the observed V···X distances (4.5 to 7 Å) have been theoretically[15] and experimentally[82,83] verified to affect T_m relaxation, but the same results have not yet been extended to T_1. This work reveals a potential effect of those same nuclei on T_1, though the effect may not be a magnetic origin from the nuclear spins themselves but rather a subtle tweaking of the crystalline lattice and local electron spin density. Future studies are necessary to better test for potential nuclear spin-based effects, nevertheless these results reveal a powerful means of changing relaxation via subtle lattice fine-tuning.

ASSOCIATED CONTENT

Supporting Information

The Supporting Information is available free of charge at https://pubs.acs.org/doi/10.1021/acs.inorgchem.5c01930.

Additional experimental details, structural data, magnetic resonance data, magnetic susceptibility data, experimental/calculated Raman spectra, and Cartesian coordination for optimized geometries of **1**−**5** (PDF)

Accession Codes

Deposition Numbers 2386039−2386040 contain the supplementary crystallographic data for this paper. These data can be obtained free of charge via the joint Cambridge Crystallographic Data Centre (CCDC) and Fachinformationszentrum Karlsruhe Access Structures service.

AUTHOR INFORMATION

Corresponding Author

Joseph M. Zadrozny − *Department of Chemistry and Biochemistry, The Ohio State University, Columbus, Ohio 43210, United States;* orcid.org/0000-0002-1309-6545; Email: Zadrozny.13@osu.edu

Authors

Roxanna Martinez − *Department of Chemistry and Biochemistry, The Ohio State University, Columbus, Ohio 43210, United States*

Ökten Üngör − *Department of Chemistry and Biochemistry, The Ohio State University, Columbus, Ohio 43210, United States*

Cassidy E. Jackson − *Department of Chemistry, Colorado State University, Fort Collins, Colorado 80523, United States*

Firoz S. T. Khan − *Department of Chemistry and Biochemistry, The Ohio State University, Columbus, Ohio 43210, United States;* orcid.org/0000-0002-3800-0423

Johan van Tol − *National High Magnetic Field Laboratory, Tallahassee, Florida 32310, United States;* orcid.org/0000-0001-6972-2149

Complete contact information is available at:

https://doi.org/10.1021/acs.inorgchem.5c01930
Inorg. Chem. 2025, 64, 15588−15599

https://pubs.acs.org/10.1021/acs.inorgchem.5c01930

Author Contributions

R.M. and C.E.J. executed the syntheses and characterization. F.S.T.K. conducted computational analyses. R.M., C.E.J., O.U., and J.v.T. conducted spectroscopic analyses. R.M. and J. Z. performed data interpretation. All authors were involved in writing the manuscript.

Notes

The authors declare no competing financial interest.

■ ACKNOWLEDGMENTS

This research was performed with partial support of Colorado State University, The Ohio State University, the National Science Foundation (2412615), and the Research Corporation for Scientific Advancement. We thank Dr. Samantha N. Macmillan at Cornell University for collecting the crystal structures of complexes **2** and **3**. A portion of this work was performed at the National High Magnetic Field Laboratory, which is supported by the National Science Foundation Cooperative Agreement No. DMR-1644779 and DMR-2128556 and the State of Florida. A portion of the work was performed with the support of The Ohio Supercomputer Center, which is a member of the Ohio Technology Consortium, a division of the Ohio Department of Higher Education.

■ REFERENCES

(1) Gatteschi, D.; Sessoli, R.; Villain, J. *Molecular Nanomagnets*; Oxford University Press, 2006.
(2) Klare, J. P. Biomedical applications of electron paramagnetic resonance (EPR) spectroscopy. *Biomed. Spectrosc. Imaging* **2012**, *1*, 101−124.
(3) Jackson, C. E.; Moseley, I. P.; Martinez, R.; Sung, S.; Zadrozny, J. A Reaction-Coordinate Perspective of Magnetic Relaxation. *Chem. Soc. Rev.* **2021**, *50*, 6684−6699.
(4) Martinez, R.; Jackson, C. E.; Üngör, Ö.; van Tol, J.; Zadrozny, J. M. Impact of ligand chlorination and counterion tuning on high-field spin relaxation in a series of V(IV) complexes. *Dalton Trans.* **2023**, *52* (31), 10805−10816.
(5) Jackson, C. E.; Ngendahimana, T.; Lin, C.-Y.; Eaton, G. R.; Eaton, S. S.; Zadrozny, J. M. Impact of Counter Ion Methyl Groups on Spin Relaxation in $[V(C_6H_4O_2)_3]^{2-}$. *J. Phys. Chem. C* **2022**, *126* (16), 7169−7176.
(6) Jackson, C. E.; Lin, C.-Y.; Johnson, S. H.; van Tol, J.; Zadrozny, J. M. Nuclear-spin-pattern control of electron-spin dynamics in a series of V(IV) complexes. *Chem. Sci.* **2019**, *10* (36), 8447−8454.
(7) Lin, C.-Y.; Ngendahimana, T.; Eaton, S. S.; Eaton, G. R.; Zadrozny, J. M. Counterion Influence on Dynamic Spin Properties in a V(IV) Complex. *Chem. Sci.* **2019**, *10* (2), 548−555.
(8) Zadrozny, J. M.; Niklas, J.; Poluektov, O. G.; Freedman, D. E. Millisecond coherence time in a tunable molecular electronic spin qubit. *ACS Cent. Sci.* **2015**, *1* (9), 488−492.
(9) Yu, C. J.; Graham, M. J.; Zadrozny, J. M.; Niklas, J.; Krzyaniak, M. D.; Wasielewski, M. R.; Poluektov, O. G.; Freedman, D. E. Long Coherence Times in Nuclear Spin-Free Vanadyl Qubits. *J. Am. Chem. Soc.* **2016**, *138* (44), 14678−14685.
(10) Bader, K.; Winkler, M.; van Slageren, J. Tuning of molecular qubits: very long coherence and spin−lattice relaxation times. *Chem. Commun.* **2016**, *52* (18), 3623−3626.
(11) Bader, K.; Dengler, D.; Lenz, S.; Endeward, B.; Jiang, S.-D.; Neugebauer, P.; van Slageren, J. Room temperature quantum coherence in a potential molecular qubit. *Nat. Commun.* **2014**, *5* (1), 5304.
(12) Bader, K.; Schlindwein, S. H.; Gudat, D.; Van Slageren, J. Molecular qubits based on potentially nuclear-spin-free nickel ions. *Phys. Chem. Chem. Phys.* **2017**, *19* (3), 2525−2529.
(13) Wolfe, J. P. Direct Observation of a Nuclear Spin Diffusion Barrier. *Phys. Rev. Lett.* **1973**, *31* (15), 907−910.
(14) Ramanathan, C. Dynamic nuclear polarization and spin diffusion in nonconducting solids. *Appl. Magn. Reson.* **2008**, *34* (3−4), 409−421.
(15) Canarie, E. R.; Jahn, S. M.; Stoll, S. Quantitative Structure-Based Prediction of Electron Spin Decoherence in Organic Radicals. *J. Phys. Chem. Lett.* **2020**, *11* (9), 3396−3400.
(16) Tan, K. O.; Mardini, M.; Yang, C.; Ardenkjær-Larsen, J. H.; Griffin, R. G. Three-spin solid effect and the spin diffusion barrier in amorphous solids. *Sci. Adv.* **2019**, *5* (7), No. eaax2743.
(17) Khutsishvili, G. R. Spin Diffusion and Magnetic Relaxation of Nuclei. *J. Exp. Theor. Phys.* **1962**, *15* (5), 909.
(18) Eaton, S. S.; Eaton, G. R. *Relaxation Mechanisms*. ; John Wiley & Sons, Ltd, 2016; Vol. 5pp 1543−1556.
(19) Aravena, D.; Ruiz, E. Spin dynamics in single-molecule magnets and molecular qubits. *Dalton Trans.* **2020**, *49* (29), 9916−9928.
(20) Llanos, L.; Aravena, D. Relaxation time enhancement by magnetic dilution in single-molecule magnets: An ab initio study. *J. Magn. Magn. Mater.* **2019**, *489*, 165456.
(21) Moseley, I. P.; Ard, C. P.; DiVerdi, J. A.; Ozarowski, A.; Chen, H.; Zadrozny, J. M. Slowing magnetic relaxation with open-shell diluents. *Cell Rep. Phys. Sci.* **2022**, *3* (3), 100802.
(22) Gatteschi, D.; Sessoli, R. Quantum Tunneling of Magnetization and Related Phenomena in Molecular Materials. *Angew. Chem., Int. Ed.* **2003**, *42* (3), 268−297.
(23) Chen, Y.-C.; Liu, J.-L.; Wernsdorfer, W.; Liu, D.; Chibotaru, L. F.; Chen, X.-M.; Tong, M.-L. Hyperfine-Interaction-Driven Suppression of Quantum Tunneling at Zero Field in a Holmium(III) Single-Ion Magnet. *Angew. Chem., Int. Ed.* **2017**, *56* (18), 4996−5000.
(24) Ishikawa, N.; Sugita, M.; Wernsdorfer, W. Nuclear Spin Driven Quantum Tunneling of Magnetization in a New Lanthanide Single-Molecule Magnet: Bis(Phthalocyaninato)holmium Anion. *J. Am. Chem. Soc.* **2005**, *127* (11), 3650−3651.
(25) Szell, P. M. J.; Bryce, D. L. Chapter Three—Recent Advances in Chlorine, Bromine, and Iodine Solid-State NMR Spectroscopy. In *Annual Reports on NMR Spectroscopy*; Webb, G. A., Ed.; Academic Press, 2015; Vol. *84*, pp 115−162.
(26) Eaton, S. S.; Eaton, G. R. Relaxation Times of Organic Radicals and Transition Metal Ions. In *Distance Measurements in Biological Systems by EPR*; Springer, 2002; pp 29−154.
(27) Ramanathan, S.; Sang, D.; Kumar, V.; Lemal, D. M. Synthesis of Tetrafluorocatechol. In *Efficient Preparations of Fluorine Compounds*; Wiley, 2012; pp 252−255.
(28) *APEX3*; Bruker AXS Inc.: Madison, Wisconsin, USA, 2012.
(29) *SADABS*; University of Göttingen: Germany, 1996.
(30) Sheldrick, G. Crystal structure refinement with SHELXL. *Acta Crystallogr., Sect. C: Struct. Chem.* **2015**, *71* (1), 3−8.
(31) Dolomanov, O. V.; Bourhis, L. J.; Gildea, R. J.; Howard, J. A. K.; Puschmann, H. OLEX2: a complete structure solution, refinement and analysis program. *J. Appl. Crystallogr.* **2009**, *42* (2), 339−341.
(32) Morley, G. W.; Brunel, L.-C.; van Tol, J. A multifrequency high-field pulsed electron paramagnetic resonance/electron-nuclear double resonance spectrometer. *Rev. Sci. Instrum.* **2008**, *79* (6), 064703.
(33) *MATLAB*. version: 9.13.0 (R2022b); The MathWorks Inc.: Natick, MA, 2022.
(34) *Origin*; OriginLab, 2018.
(35) Stoll, S.; Schweiger, A. EasySpin, a comprehensive software package for spectral simulation and analysis in EPR. *J. Magn. Reson.* **2006**, *178* (1), 42−55.
(36) Kazmierczak, N. P.; Lopez, N. E.; Luedecke, K. M.; Hadt, R. G. Determining the key vibrations for spin relaxation in ruffled Cu(II) porphyrins via resonance Raman spectroscopy. *Chem. Sci.* **2024**, *15* (7), 2380−2390.
(37) Becke, A. D. Density-functional thermochemistry. III. The role of exact exchange. *J. Chem. Phys.* **1993**, *98* (7), 5648−5652.

(38) Lee, C.; Yang, W.; Parr, R. G. Development of the Colle-Salvetti correlation-energy formula into a functional of the electron density. *Phys. Rev. B* **1988**, *37* (2), 785−789.
(39) Stephens, P. J.; Devlin, F. J.; Chabalowski, C. F.; Frisch, M. J. Ab Initio Calculation of Vibrational Absorption and Circular Dichroism Spectra Using Density Functional Force Fields. *J. Phys. Chem.* **1994**, *98* (45), 11623−11627.
(40) *Gaussian 16*; Gaussian, Inc.: Wallingford, CT, 2016.
(41) *Ohio Supercomputer Center*, 1987.
(42) ChemCraft. *Graphical Software for Visualization of Quantum Chemistry Computations*, 2025.
(43) Bulls, A. R.; Pippin, C. G.; Hahn, F. E.; Raymond, K. N. Synthesis and characterization of a series of vanadium-tunichrome B1 analogs. Crystal structure of a tris(catecholamide) complex of vanadium. *J. Am. Chem. Soc.* **1990**, *112* (7), 2627−2632.
(44) Cooper, S. R.; Koh, Y. B.; Raymond, K. N. Synthetic, structural, and physical studies of bis(triethylammonium) tris(catecholato)-vanadate(IV), potassium bis(catecholato)oxovanadate(IV), and potassium tris(catecholato)vanadate (III). *J. Am. Chem. Soc.* **1982**, *104* (19), 5092−5102.
(45) Schindler, M.; Hawthorne, F. C.; Baur, W. H. Crystal Chemical Aspects of Vanadium: Polyhedral Geometries, Characteristic Bond Valences, and Polymerization of (VO_n) Polyhedra. *Chem. Mater.* **2000**, *12* (5), 1248−1259.
(46) Zanello, P.; Corsini, M. Homoleptic mononuclear transition metal complexes of 1,2-dioxolenes: Updating their electrochemical-to-structural (X-ray) properties. *Coord. Chem. Rev.* **2006**, *250* (15−16), 2000−2022.
(47) Zecevic, A.; Eaton, G. R.; Eaton, S. S.; Lindgren, M. Dephasing of electron spin echoes for nitroxyl radicals in glassy solvents by non-methyl and methyl protons. *Mol. Phys.* **1998**, *95* (6), 1255−1263.
(48) Goldfarb, D.; Stoll, S. *EPR Spectroscopy: Fundamentals and Methods*; Wiley, 2018.
(49) Spikes, G. H.; Sproules, S.; Bill, E.; Weyhermüller, T.; Wieghardt, K. One- and Two-Electron Reduced 1,2-Diketone Ligands in $[Cr^{III}(L^{\bullet})_3]$ (S = 0) and $Na_2(Et_2O)_2[V^{IV}(L^{Red})_3]$ (S = 1/2). *Inorg. Chem.* **2008**, *47* (23), 10935−10944.
(50) Chun, H.; Verani, C. N.; Chaudhuri, P.; Bothe, E.; Bill, E.; Weyhermüller, T.; Wieghardt, K. Molecular and Electronic Structure of Octahedral o-Aminophenolato and o-Iminobenzosemiquinonato Complexes of V(V), Cr(III), Fe(III), and Co(III). Experimental Determination of Oxidation Levels of Ligands and Metal Ions. *Inorg. Chem.* **2001**, *40* (17), 4157−4166.
(51) Diamantis, A. A.; Raynor, J. B.; Rieger, P. H. Re-examination of the electron spin resonance spectrum of trigonal-prismatic bis-[pentane-2,4-dione benzoylhydrazonato(2−)]vanadium(IV). *J. Chem. Soc., Dalton Trans.* **1980**, No. 9, 1731−1733.
(52) Zadrozny, J. M.; Niklas, J.; Poluektov, O. G.; Freedman, D. E. Multiple quantum coherences from hyperfine transitions in a vanadium(IV) complex. *J. Am. Chem. Soc.* **2014**, *136* (45), 15841−15844.
(53) Matsubayashi, G.; Akiba, K.; Tanaka, T. Spectroscopic and electrical properties of $VO(dmit)_2$ and $V(dmit)_3$ anion complexes and x-ray crystal structure of $[NMP]_2[V(dmit)_3]$ (dmit = 2-thioxo-1,3-dithiole-4,5-dithiolate, NMP = N-methylphenazinium). *Inorg. Chem.* **1988**, *27* (26), 4744−4749.
(54) Olk, R.-M.; Dietzsch, W.; Kirmse, R.; Stach, J.; Hoyer, E.; Golič, L. (III), Tl(III) and V(IV) tris-chelates of the heterocyclic dithiolene and diselenolene ligands 1,3-dithiole-2-thione-4,5-dithiolate (dmit), 1,2-dithiole-3-thione-4,5-dithiolate (dmt) and 1,3-diselenole-2-selone-4,5-diselenolate (dsis). Crystal and molecular structure of $(Bu_4N)_2$ [V(dmt)3]. *Inorg. Chim. Acta* **1987**, *128* (2), 251−259.
(55) Branca, M.; Micera, G.; Dessi, A.; Sanna, D.; Raymond, K. N. Formation and structure of the tris(catecholato)vanadate(IV) complex in aqueous solution. *Inorg. Chem.* **1990**, *29* (8), 1586−1589.
(56) Schweiger, A.; Jeschke, G. *Principles of Pulse Electron Paramagnetic Resonance*; Oxford University Press, 2001; ..
(57) Schäfter, D.; Wischnat, J.; Tesi, L.; De Sousa, J. A.; Little, E.; McGuire, J.; Mas-Torrent, M.; Rovira, C.; Veciana, J.; Tuna, F.; et al. Molecular One- and Two-Qubit Systems with Very Long Coherence Times. *Adv. Mater.* **2023**, *35* (38), 2302114.
(58) Tesi, L.; Lunghi, A.; Atzori, M.; Lucaccini, E.; Sorace, L.; Totti, F.; Sessoli, R. Giant spin−phonon bottleneck effects in evaporable vanadyl-based molecules with long spin coherence. *Dalton Trans.* **2016**, *45* (42), 16635−16643.
(59) Stinghen, D.; Atzori, M.; Fernandes, C. M.; Ribeiro, R. R.; de Sá, E. L.; Back, D. F.; Giese, S. O. K.; Hughes, D. L.; Nunes, G. G.; Morra, E.; et al. A Rare Example of Four-Coordinate Nonoxido Vanadium(IV) Alkoxide in the Solid State: Structure, Spectroscopy, and Magnetization Dynamics. *Inorg. Chem.* **2018**, *57* (18), 11393−11403.
(60) Santanni, F.; Albino, A.; Atzori, M.; Ranieri, D.; Salvadori, E.; Chiesa, M.; Lunghi, A.; Bencini, A.; Sorace, L.; Totti, F.; et al. Probing Vibrational Symmetry Effects and Nuclear Spin Economy Principles in Molecular Spin Qubits. *Inorg. Chem.* **2021**, *60* (1), 140−151.
(61) Atzori, M.; Tesi, L.; Benci, S.; Lunghi, A.; Righini, R.; Taschin, A.; Torre, R.; Sorace, L.; Sessoli, R. Spin Dynamics and Low Energy Vibrations: Insights from Vanadyl-Based Potential Molecular Qubits. *J. Am. Chem. Soc.* **2017**, *139* (12), 4338−4341.
(62) Atzori, M.; Benci, S.; Morra, E.; Tesi, L.; Chiesa, M.; Torre, R.; Sorace, L.; Sessoli, R. Structural Effects on the Spin Dynamics of Potential Molecular Qubits. *Inorg. Chem.* **2018**, *57* (2), 731−740.
(63) Fataftah, M. S.; Krzyaniak, M. D.; Vlaisavljevich, B.; Wasielewski, M. R.; Zadrozny, J. M.; Freedman, D. E. Metal-ligand covalency enables room temperature molecular qubit candidates. *Chem. Sci.* **2019**, *10* (27), 6707.
(64) Atzori, M.; Morra, E.; Tesi, L.; Albino, A.; Chiesa, M.; Sorace, L.; Sessoli, R. Quantum Coherence Times Enhancement in Vanadium(IV)-based Potential Molecular Qubits: the Key Role of the Vanadyl Moiety. *J. Am. Chem. Soc.* **2016**, *138* (35), 11234−11244.
(65) Jackson, C. E.; Lin, C.-Y.; van Tol, J.; Zadrozny, J. M. J. M. Orientation dependence of phase memory relaxation in the V(IV) ion at high frequencies. *Chem. Phys. Lett.* **2020**, *739*, 137034.
(66) Espinosa, M. R.; Guerrero, F.; Kazmierczak, N. P.; Oyala, P. H.; Hong, A.; Hadt, R. G.; Agapie, T. Slow Electron Spin Relaxation at Ambient Temperatures with Copper Coordinated by a Rigid Macrocyclic Ligand. *J. Am. Chem. Soc.* **2025**, *147* (17), 14036−14042.
(67) Van Vleck, J. H. Paramagnetic Relaxation Times for Titanium and Chrome Alum. *Phys. Rev.* **1940**, *57* (5), 426−447.
(68) De Vroomen, A. C.; Lijphart, E. E.; Prins, D. Y. H.; Marks, J.; Poulis, N. J. Electron spin-lattice relaxation of the Zeeman and interaction systems in $CuCs_2(SO_4)_2{\cdot}6H_2O$. *Physica* **1972**, *61* (2), 241−249.
(69) De Vroomen, A. C.; Lijphart, E. E.; Poulis, N. J. Electron spin-lattice relaxation of Cu++ in zinc ammonium tutton salt. *Physica* **1970**, *47* (3), 458−484.
(70) De Vries, A. J.; Curtis, D. A.; Livius, J. W. M.; Van Duyneveldt, A. J.; Gorter, C. J. Spin-lattice relaxation in a few hydrated paramagnetic sulphates. *Physica* **1967**, *36* (1), 91−106.
(71) Atzori, M.; Tesi, L.; Morra, E.; Chiesa, M.; Sorace, L.; Sessoli, R. Room-Temperature Quantum Coherence and Rabi Oscillations in Vanadyl Phthalocyanine: Toward Multifunctional Molecular Spin Qubits. *J. Am. Chem. Soc.* **2016**, *138* (7), 2154−2157.
(72) Mirzoyan, R.; Kazmierczak, N. P.; Hadt, R. G. Deconvolving Contributions to Decoherence in Molecular Electron Spin Qubits: A Dynamic Ligand Field Approach. *Chem.—Eur. J.* **2021**, *27* (37), 9482−9494.
(73) Mirzoyan, R.; Hadt, R. G. The dynamic ligand field of a molecular qubit: decoherence through spin−phonon coupling. *Phys. Chem. Chem. Phys.* **2020**, *22* (20), 11249−11265.
(74) Kazmierczak, N. P.; Mirzoyan, R.; Hadt, R. G. The Impact of Ligand Field Symmetry on Molecular Qubit Coherence. *J. Am. Chem. Soc.* **2021**, *143* (42), 17305−17315.
(75) Amdur, M. J.; Mullin, K. R.; Waters, M. J.; Puggioni, D.; Wojnar, M. K.; Gu, M.; Sun, L.; Oyala, P. H.; Rondinelli, J. M.; Freedman, D. E. Chemical control of spin−lattice relaxation to

https://doi.org/10.1021/acs.inorgchem.5c01930
Inorg. Chem. 2025, 64, 15588−15599

discover a room temperature molecular qubit. *Chem. Sci.* **2022**, *13* (23), 7034−7045.
(76) Hardcastle, F. D.; Wachs, I. E. Determination of vanadium-oxygen bond distances and bond orders by Raman spectroscopy. *J. Phys. Chem.* **1991**, *95* (13), 5031−5041.
(77) Solomon, E. I.; Lever, A. B. P. *Inorganic Electronic Structure and Spectroscopy*; John Wiley & Sons: New York, 1999; Vol. 2.
(78) Graham, M. J.; Zadrozny, J. M.; Fataftah, M. S.; Freedman, D. E. Forging Solid-State Qubit Design Principles in a Molecular Furnace. *Chem. Mater.* **2017**, *29* (5), 1885−1897.
(79) Ryan, C.; Briganti, V.; Hogan, C.; O'Neill, M.; Lunghi, A. Spin decoherence in molecular crystals: nuclear v.s. electronic spin baths. *arXiv* **2025**, arXiv: 2504.18254.
(80) Murphy, J. Spin-Lattice Relaxation Due to Local Vibrations with Temperature-Independent Amplitudes. *Phys. Rev.* **1966**, *145* (1), 241−247.
(81) Aruachan, K.; Colón, Y. J.; Aravena, D.; Herrera, F. Semi-empirical Haken−Strobl model for molecular spin qubits. *New J. Phys.* **2023**, *25*, 093031.
(82) Graham, M. J.; Yu, C.-J.; Krzyaniak, M. D.; Wasielewski, M. R.; Freedman, D. E. Synthetic Approach To Determine the Effect of Nuclear Spin Distance on Electronic Spin Decoherence. *J. Am. Chem. Soc.* **2017**, *139* (8), 3196−3201.
(83) Graham, M. J.; Krzyaniak, M. D.; Wasielewski, M. R.; Freedman, D. E. Probing Nuclear Spin Effects on Electronic Spin Coherence via EPR Measurements of Vanadium(IV) Complexes. *Inorg. Chem.* **2017**, *56* (14), 8106−8113.

https://doi.org/10.1021/acs.inorgchem.5c01930
Inorg. Chem. 2025, 64, 15588−15599